doi: 10.56761/EFRE2022.C4-O-037801

Tailoring of optical, mechanical and surface properties of high-entropy ceramic thin films

S. Zenkin[*], *A. Gaydaychuk, A. Mitulinsky, S. Linnik*

Tomsk Polytechnic University, Tomsk, Russia
[*]*zen@tpu.ru*

Abstract. In this article we show the optical, mechanical and surface properties change depending on the Hf-Zr-Ce-Y-O thin film composition. $Hf_4Zr_4CeY_2O_{21}$ shows up to three times higher hardness compared to binary $HfZrO_4$ oxide and up to 50% higher hardness compared to cubic ZrO_2 and HfO_2 due to the solid solution hardening effect. Equimolar film exhibit a high transmittance >85% and high hydrophobicity with the water contact angle ≈106°. Variation of the elemental composition in Hf-Zr-Ce-Y-O is allows to simultaneously tune mechanical and wetting properties for the optimum configuration depending on the application.
Keywords: high entropy oxide, HiPIMS, mechanical properties, hydrophobic ceramics.

1. Introduction

Materials with a combination of high hydrophobicity, enhanced mechanical properties (hardness, toughness) and thermal stability find a various application such as aircraft protection from the ice formation [1] or dropwise condensation heat transfer [2]. Most of the studies which are focused on these applications are deal with polymer materials and trying to find a way of their mechanical properties enhancement [3–5]. Report about the rare earth oxides hydrophobicity shows that these ceramics exhibit excellent combination of the water contact angle ($\theta > 90°$) and high mechanical properties [6]. Subsequent works show that the group of the low-electronegativity metals oxides also exhibit the hydrophobic effect [7]. Previously we showed that it is possible to enhance the mechanical properties of this group of ceramics without a weakening of the hydrophobic effect [8]. Several methods of the mechanical properties enhancement can be used for non-polymer thin films [9, 10]. One of the most promising is the entropy stabilization. The conception of the entropy stabilization of the solid crystal structure was received a wide attention in the past decade due to superior and tunable properties of reported high entropy materials [11]. High entropy alloys are surpassing traditional alloys and compounds in thermal stability [12] and mechanical properties [13], making them a potential high-performance constructive and functional materials [14]. A high entropy material is a solid solution of four-, five- or more components with a simple crystal structure, usually BCC or FCC [11]. Thermodynamic stability of this solid solution is given by the minimization of the Gibbs free energy:

$$\Delta G_{mix} = \Delta H_{mix} - T\Delta S_{mix}, \quad (1)$$

here, ΔG_{mix} is the Gibbs free energy of mixing, ΔH_{mix} is the enthalpy of mixing, ΔS_{mix} is the entropy of mixing, and T is the absolute temperature.

An entropy of the system is described using the Boltzmann's equation:

$$\Delta S_{mix} = -R\sum_i c_i \ln(c_i), \quad (2)$$

here, R is the gas constant, and c_i is the molar content of the component.

Resulted Gibbs free energy from the equation (1) is minimized by the enlarged entropy of mixing with the value up to $\Delta S_{mix} = 1.61R$ for a five-component materials in comparison with traditional materials, giving an additional thermodynamic stabilization of the system [14]. Up to date, main researches were focused on the high entropy metallic systems (high entropy alloys or HEA). Recently Rost et al. show that entropy stabilization concept is also applicable for ceramic systems [15]. Subsequent works have discovered other properties of this class of materials such as

high oxidation resistance [16], superhardness [17] or advanced superionic conductivity [18]. This remarkable improvement of material properties led to the suggestion that entropic stabilization is also applicable for the UHTC ceramics production, where the reduced Gibbs free energy can lead to the higher thermal stability of solids [19].

In order to create a robust transparent hydrophobic ceramics for the selection of the high entropy oxide (HEO) composition we used the combination of three material properties: a high melting temperature of the oxide, the lowest enthalpy of formation (or minimum Gibbs free energy per mole O_2) and low electronegativity of the base element. Resulted group of the selected oxides was taken as HfO_2, ZrO_2, Y_2O_3 and CeO_2, excluding radioactive ThO_2 and PuO_2 and toxic BeO (Fig.1a). MgO was excluded due to the reduced thermal stability at temperatures higher than 1400°C. While an incorporation of the La_2O_3 as a fifth component can lead to the formation of the binary pyrochlore structures like $La_2Zr_2O_7$ and $La_2Hf_2O_7$ [20].

Also, the HfO_2-ZrO_2-CeO_2 system is characterized by a positive value of the mixing enthalpy (ΔH_{mix} = +51.0 ± 8.0 kJ/mol for the equimolar ZrO_2-CeO_2 composition [21]) leading to a possibility of a phase separation and surface segregation to zirconium-rich and cerium-rich regions [22], contrary to the HfO_2-ZrO_2-Y_2O_3 system, which is characterized by the ΔH_{mix} = 0 (ideal solid solution) for all molar ratios. Resulted composition of HEO $HfZrCeYO_{2-\delta}$ is characterized by the entropy value $\Delta S_{mix} = 1.38R$ and a simple cubic Fm-3 m structure (Fig.1b). Use of the entropic stabilization allows us to achieve a following superior combination of characteristics:

1) An addition of CeO_2 and Y_2O_3 is stabilize the high temperature hard cubic structure of ZrO_2 and HfO_2 without a phase transformation from the room temperature up to the melting temperature T_m [23].

2) Minimization of the Gibbs free energy of the HEO system gives an additional thermodynamic stability.

3) Formation of a simple solid solution of the cubic oxides with T_m > 2000°C excluding formation of binary oxides.

4) HEO mechanical properties enhancement due to the solid solution hardening effect [24].

5) Due to the low electronegativity of constituent elements (Hf, Zr, Y, Ce) we expect the high hydrophobicity of synthesized HEO oxides [6, 7].

The main goal of this study is to investigate the relation between the mechanical, optical and hydrophobic properties of HEO system Hf-Zr-Ce-Y-O in dependance on the elemental composition.

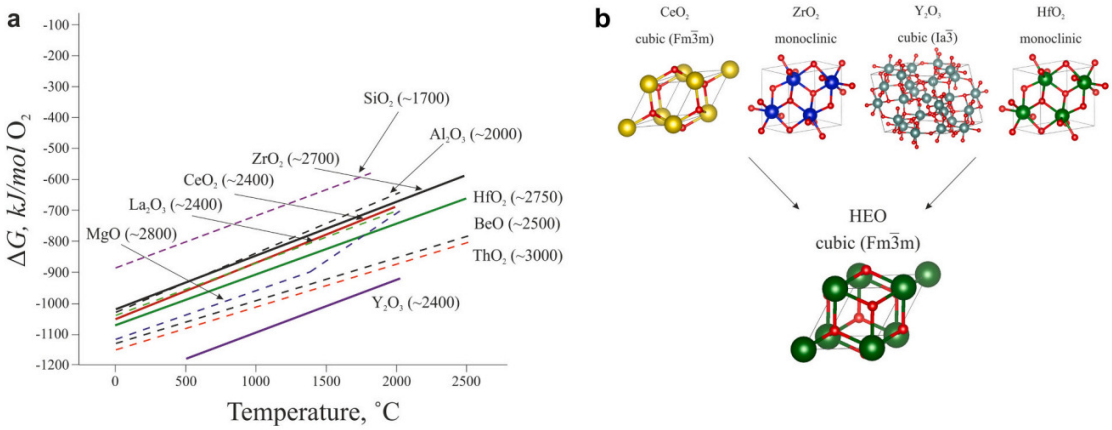

Fig.1. Ellingham diagrams of the most thermally stable oxides with respective melting temperatures (a), here solid lines are selected oxides and dashed lines are excluded oxides in this study; crustal structures of the selected component oxides at the ambient conditions and resulted crystal structure of the high entropy oxide $HfZrCeYO_{2-\delta}$ (b).

2. Material and methods

Several substrates for the measurements were used:

1) A monocrystalline Si(100) with the size of 15×15×0.38 mm for XRD, SEM and mechanical properties measurements;

2) A monocrystalline Si(100) with the size of 35×5×0.38 mm for the stress measurements;

3) A glass with the size of 15×15×1 mm for the optical absorption properties measurements.

Before placing to the vacuum chamber samples were ultrasonically cleaned in acetone and isopropyl alcohol. High entropy oxide films were sputtered using two round unbalanced magnetrons equipped with HfZr (50/50 at.%) and CeY (33/66 at.%) targets. Target diameter was 100 mm. Purity of the targets were 99.95%. The magnetrons were powered by high power impulse magnetron sputtering (HiPIMS) power supply (1 kV, 5 kW, Applied Electronics, Russia). At the initial stage samples were cleaned by the Ar^+ ion source with the energy of 1.5 keV. The base pressure p_0 in the evacuated chamber was $8 \cdot 10^{-4}$ Pa. The $HfZrCeYO_{2-\delta}$ films were deposited on substrate under the following conditions: discharge voltage U_d = 700–900 V, pulse period τ = 50 μs, pulse frequency f = 1 kHz, substrate temperature T_s = 300 °C, substrate-to-target distance d_{s-t} = 100 mm, argon pressure p_{Ar} = 0.5 Pa and oxygen pressure p_{O2} = 0.5 Pa. Molar concentration in the growing films was controlled by the power ratio on the magnetron targets with the range of 0.5–2 kW. Coatings surface, cross-sectional morphology and elemental composition were studied using a scanning electron microscope (Quanta SEM, Thermo Scientific). Structural characteristics of the coatings were studied using X-ray diffraction (Shimadzu XRD 6000) instrument with Cu Kα (λ = 0.154 nm) radiation. Samples curvature was measured by the optical profilometer (Micro Measure 3D Station, STIL) and film stress was calculated from the curvature measurements by using the Stoney formula. Optical properties of as-deposited coatings were characterized by their optical density measured by an optical absorption spectroscopy using the AvaSpec-3648 spectrometer operated at wavelengths ranging from 350 to 850 nm.

3. Results and discussion

3.1. Elemental composition and film structure

In order to prepare a complex HEO system we used a reactive high power impulse magnetron sputtering technique (r-HiPIMS). In this technique highly ionized fluxes of particles onto substrate with a high percentage of metal ions and enlarged ion energies bombarding the substrate are allow to grow dense homogeneous oxide films. Film's composition was controlled by the variation of an average power ratio on the HfZr and CeY targets during the co-sputtering in argon-oxygen atmosphere. Firstly, for the properties comparison we prepared binary $Ce_3Y_4O_{12}$ and $HfZrO_4$ films, Fig.2a. Sputtered binary oxides are characterized by the cubic structure for $Ce_3Y_4O_{12}$ and the mixed cubic+monoclinic structure for $HfZrO_4$ without preferred orientation (Fig.2a, blue and orange lines respectively). Contrary, HEO films are characterized by the cubic Fm-3 m structure with XRD peaks shifted proportionally to the increase of the molar HfZr concentration in agreement with the Vegard's law [25]. Resulted 2θ peak shift is in the range of 1.29° for (1 1 1) and up to 3.06° for (3 1 1). Preferred orientation of sputtered HEO films is transformed from (1 1 1) to (2 0 0) plane with the growth of the HfZr concentration (Fig.2a). However, we attribute these changes not to the HfZr concentration growth itself, but rather the influence of the high-energy particles bombardment of the growing film from the HfZr target due to the enlarged average target power density [26]. We cannot detect any phase separation for all synthesized $HfZrCeYO_{2-\delta}$ films. A cubic Fm-3 m structure of $HfZrCeYO_{2-\delta}$ not divides to separated mono- or binary oxides in a wide range of molar compositions. EDS mapping of the representative $Hf_2Zr_2CeY_2O_{13}$ film shows the homogeneous distribution of all constituent elements without any local elements segregation and phase separation to the Me-rich regions, Fig.2c.

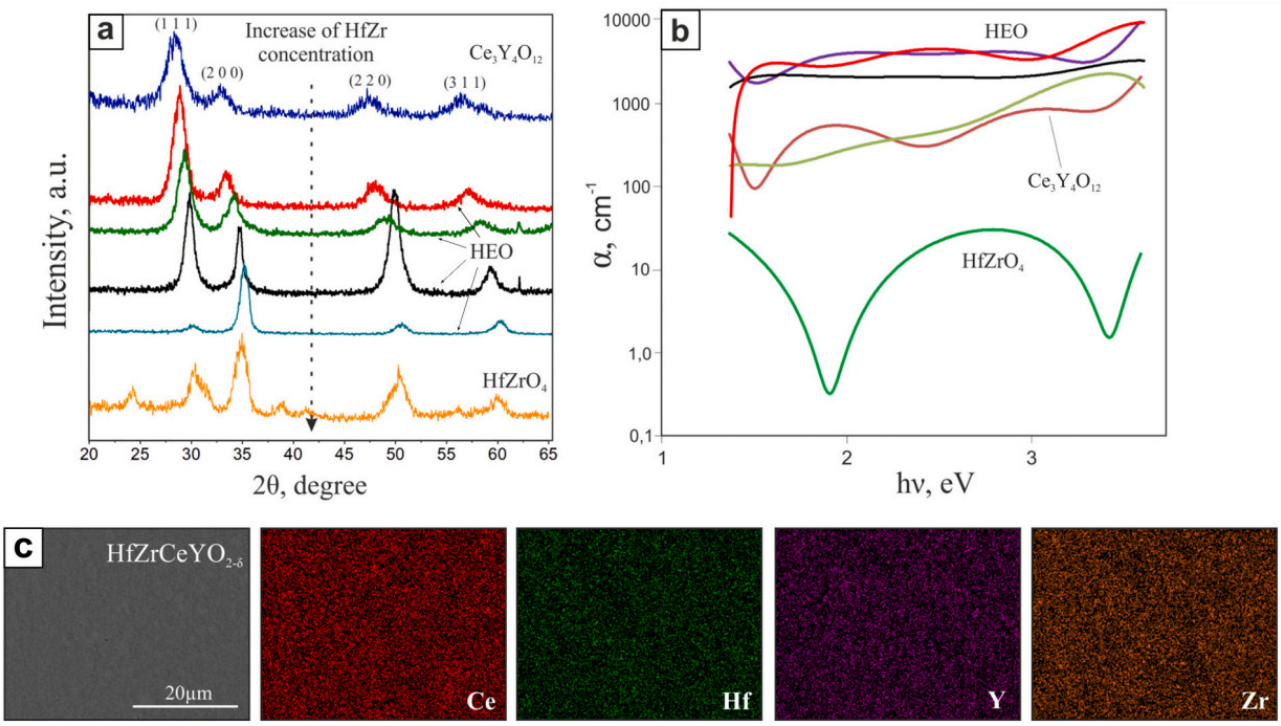

Fig.2. XRD patterns of $Ce_3Y_4O_{12}$ (blue), $HfZrO_4$ (orange), HEO: $Hf_{0.5}Zr_{0.5}CeY_2O_7$ (red), $HfZrCeY_2O_9$ (green), $Hf_2Zr_2CeY_2O_{13}$ (black), $Hf_4Zr_4CeY_2O_{21}$ (light blue) (a); Spectral dependence of the absorption coefficient of $HfZrO_4$ (green), $Ce_3Y_4O_{12}$ (brown), $Hf_{0.5}Zr_{0.5}CeY_2O_7$ (light green), $HfZrCeY_2O_9$ (red), $Hf_2Zr_2CeY_2O_{13}$ (black), $Hf_4Zr_4CeY_2O_{21}$ (b); top view SEM of the $Hf_2Zr_2CeY_2O_{13}$ and the corresponding EDS mapping of each composition element (c).

The presence of a 3+ valence yttrium cation [27] in the $HfZrCeYO_{2-\delta}$ composition leading to the formation of oxygen vacancies and crystal defects generation and hence absorption centers concentration growth during the formation of the solid solution. In order to estimate this factor we measured optical absorption properties of the sputtered HEO films, Fig.2b. The spectral dependence of the absorption coefficient was calculated as:

$$\alpha(h\upsilon) = D(h\upsilon)/d\,, \tag{3}$$

here $D(h\upsilon)$ is a spectral characteristic of the optical density and d is the film thickness.

$HfZrO_4$ films are characterized by the minimum of the light absorption centers concentration for all synthetized films with the characteristic absorption value around 2.8 eV, due to the ordered crystalline structure, Fig.2b. Contrary, $Ce_3Y_4O_{12}$ exhibited in order of magnitude higher value of light absorption centers concentration. A transfer from the $Ce_3Y_4O_{12}$ to the $HfZrO_4$ by an addition of the HfZr is characterized by the formation of $HfZrCeYO_{2-\delta}$ composition with a higher absorption centers concentration, leading to the growth the absorption coefficient in order of magnitude. Distribution of these centers is homogeneous for the whole measurement interval for $HfZrCeYO_{2-\delta}$ compositions from $HfZrCeY_2O_9$ to $Hf_4Zr_4CeY_2O_{21}$. This distribution is a fact of a maximum structure disorder and formation of a nanocrystalline structure [28].

Despite the fact that synthesized HEO films exhibit a high absorption centers concentration, their transmittance is relatively high, Fig.3a and 3d. For the light wavelength 550 nm the transmittance of the 2800 nm thick $Hf_2Zr_2CeY_2O_{13}$ film is around 85% while for 500 nm thick $Hf_2Zr_2CeY_2O_{13}$ film transmittance is around 90%, comparable with an uncoated glass substrate. SEM cross-section measurements show a glass-like structure without pronounced crystalline structure (in agreement with the measured absorption centers distribution) for all synthesized HEO

films for the group $HfZrCeY_2O_9$ - $Hf_4Zr_4CeY_2O_{21}$, Fig.3b. The measured roughness R_a was in the range of 2.5–3.6 nm. This minor variation of the films roughness allows us do not take it into account during the surface measurements, described below.

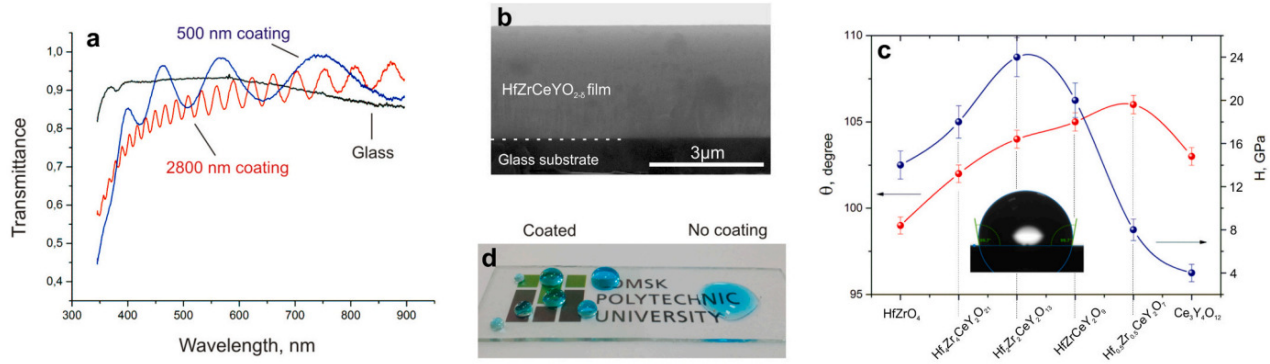

Fig.3. a) Transmittance measurements of the silica glass (black), coated by 500 nm $Hf_2Zr_2CeY_2O_{13}$ HEO (blue) and coated by 2800 nm $Hf_2Zr_2CeY_2O_{13}$ HEO (red); b) cross-section SEM image of the $Hf_2Zr_2CeY_2O_{13}$ HEO film on the glass substrate; c) WDCA and hardness in dependence of the $HfZrCeYO_{2-\delta}$ film composition; d) water wetting of silica glass partially coated by 2800 nm $Hf_2Zr_2CeY_2O_{13}$ HEO film.

3.2. Surface properties of $HfZrCeYO_{2-\delta}$ films

Surface properties of sputtered films were determined by use of the van Oss-Good-Chaudhury equation [29]:

$$\gamma_L(1+\cos\theta) = 2\left(\sqrt{\gamma_S^{LW}\gamma_L^{LW}} + \sqrt{\gamma_S^{+}\gamma_L^{-}} + \sqrt{\gamma_S^{-}\gamma_L^{+}}\right). \quad (4)$$

Here θ is the contact angle with a droplet of liquid L, γ_S^{LW} is the electrostatic Lifshitz-van der Waals component of the surface free energy of the solid film, and γ_S^{+} and γ_S^{-} are, respectively, the polar Lewis acid and the polar Lewis base components giving the polar acid-base component γ_S^{AB} as:

$$\gamma_S^{AB} = 2\sqrt{\gamma_S^{+}\gamma_L^{-}}\,. \quad (5)$$

The total surface free energy of the film γ_S is then given as the sum of the Lifshitz-van der Waals and the polar acid-base component:

$$\gamma_{total} = \gamma^{LW} + \gamma^{AB}\,. \quad (6)$$

As a testing liquids we used water, glycerol and α – bromonaphthalene.

Results of the measurement are presented in Fig.3c and Table 1. All synthesized films exhibited ≈98% of the electrostatic Lifshitz-van der Waals interaction with water in agreement with previous studies [6, 7]. On can see that the total surface energy γ_{total} for $HfZrCeYO_{2-\delta}$ films decreases with the increasing of the Ce–Y concentration from 40.33 mJ/m^2 for $HfZrO_4$ to 32.58 mJ/m^2 for $Ce_3Y_4O_{12}$. The corresponding water contact angle increases from ≈98° for the $HfZrO_4$ to ≈102° for the $Ce_3Y_4O_{12}$. It is important to note that the maximum of the contact angle ≈106° and the minimum of the surface energy $\gamma_{total} = 31.29$ mJ/m^2 was measured for the $Hf_{0.5}Zr_{0.5}CeY_2O_7$ composition.

3.2. Mechanical properties of $HfZrCeYO_{2-\delta}$ films

Mechanical properties of as-prepared $HfZrCeYO_{2-\delta}$ films are summarized in Table 2. All films exhibited a relatively low residual compressive stress σ less than – 1.5 GPa and a high elastic recovery W_e > 60%. Hardness H and Young's modulus E^* continuously increase with the shift from

binary oxides $Ce_3Y_4O_{12}$ and $HfZrO_4$ to the equimolar $HfZrCeYO_{2-\delta}$ composition with a maximum hardness of H = 22.4 GPa for the $Hf_4Zr_4CeY_2O_{21}$. Also, for the $HfZrCeYO_{2-\delta}$ film group $HfZrCeY_2O_9$ - $Hf_4Zr_4CeY_2O_{21}$ one can detect a high ratio of H/E^* > 0.1, which is in combination with a high elastic recovery W_e > 60% gives an enhanced resistance to cracks formation [30]. $HfZrCeYO_{2-\delta}$ shows up to three times higher hardness in comparison with binary $HfZrO_4$ oxide and up to 50% higher hardness in comparison with cubic ZrO_2 and HfO_2 [31].

Table 1. Surface free energies of $HfZrCeYO_{2-\delta}$ HEO films. Here γ_{total} is the total surface free energy equal to the sum of the non-polar Lifshitz-van der Waals component γ^{LW} and the polar acid-base component γ^{AB}

$HfZrCeYO_{2-\delta}$ film composition	**γ_{total} [mJ/m^2]**	**γ^{LW} [mJ/m^2]**	**γ^{AB} [mJ/m^2]**
$HfZrO_4$	40.33	39.99	0.34
$Hf_4Zr_4CeY_2O_{21}$	36.24	35.80	0.44
$Hf_2Zr_2CeY_2O_{13}$	33.01	32.51	0.50
$HfZrCeY_2O_9$	31.70	30.95	0.75
$Hf_{0.5}Zr_{0.5}CeY_2O_7$	31.29	31.07	0.22
$Ce_3Y_4O_{12}$	32.58	31.66	0.92

Table 2. Mechanical properties of the synthesized $HfZrCeYO_{2-\delta}$ films

Elemental composition	***H* [GPa]**	***E** [GPa]**	**W_e [%]**	***H/E****	**σ [GPa]**
$Ce_3Y_4O_{12}$	4.9	79.3	60	0.062	–0,5
$Hf_{0.5}Zr_{0.5}CeY_2O_7$	17.3	180.6	66	0.096	–0,7
$HfZrCeY_2O_9$	19.7	187.6	67	0.105	–0,9
$Hf_2Zr_2CeY_2O_{13}$	21.3	196.7	69	0.108	–1,3
$Hf_4Zr_4CeY_2O_{21}$	22.4	194.8	71	0.115	–1,2
$HfZrO_4$	7.7	110.3	62	0.070	–0,9

We attribute this enhancement to the solid solution hardening effect (that is typical for the high entropy alloys family [32]), where the atomic scale solid solution dependent lattice distortion gives a significant intrinsic friction stress (i.e., Peierls stress) with an enhanced hardness and strength [24]. Also, the hardness of the equimolar $Hf_2Zr_2CeY_2O_{13}$ films reported in this work is significantly higher than reported by the J. Gild et al. for the bulk $(Hf_{0.25}Zr_{0.25}Ce_{0.25}Y_{0.25})O_{2-\delta}$ with the hardness of H = 13.6 GPa [33]. These differences can be given by the Hall-Petch effect, similar to other nanocrystalline thin film materials [34]. However, the hardness of the HEO is still lower in comparison with high entropy nitrides [35, 36], similarly to the hardness relation between the simple binary oxides and nitrides of the same element.

4. Conclusion

Based on the measured data we can conclude that:

1) The $HfZrCeYO_{2-\delta}$ system form a solid solution with the simple cubic (Fm-3 m) structure without formation of binary oxides and an absence of the phase separation.

2) Hardness in the Hf-Zr-Ce-Y-O system shows nonlinear character in dependence on the molar composition. $Hf_4Zr_4CeY_2O_{21}$ shows up to three times higher hardness (H = 22GPa) in comparison to binary $HfZrO_4$ oxide and up to 50% higher hardness in comparison with cubic ZrO_2 and HfO_2 due to the solid solution hardening effect.

3) Absorption centers distribution in the high entropy oxides shows a homogeneous character and is in order of magnitude higher in comparison with the binary oxides. We suggest that this criterion can be a signature of HEO materials. However, the transmittance of the $Hf_2Zr_2CeY_2O_{13}$ film is around 85%.

4) Hf-Zr-Ce-Y-O system shows a high hydrophobic effect with the maximum contact angle for the $Hf_{0.5}Zr_{0.5}CeY_2O_7$ composition is ≈106°.

Acknowledgement

The study was supported by RFBR, project number 19-29-13034. The thin films growth equipment was created with the support by Tomsk Polytechnic University development program.

5. References

[1] Piscitelli F., Chiariello A., Dabkowski D., Corraro G., Marra F., Di Palma L., *Aerospace*, **7**(1), 2, 2020; doi: 10.3390/aerospace7010002
[2] Liu L., Wang S., Zeng X., Pi P., Wen X., *Adv. Mater. Interfaces*, 2101603, 2021; doi: 10.1002/admi.202101603
[3] Hoshian S., Jokinen V., Somerkivi V., Lokanathan A.R., Franssila S., *ACS Appl. Mater. Interfaces*, **7**(1), 941, 2015; doi: 10.1021/am507584j
[4] Lu Y., Sathasivam S., Song J., Crick C.R., Carmalt C.J., Parkin I.P., *Science*, **347**, 1132, 2015; doi: 10.1126/science.aaa0946
[5] Zhang W., Xiang T., Liu F., Zhang M., Gan W., Zhai X., Di X., Wang Y., Liu G., Wang C., *ACS Appl. Mater. Interfaces*, **9**, 15776, 2017; doi: 10.1021/acsami.7b02158
[6] Azimi G., Dhiman R., Kwon H.-M., Paxson A.T., Varanasi K.K., *Nat. Mater.*, **12**, 315, 2013; doi: 10.1038/nmat3545
[7] Zenkin S., Kos S., Musil J., *J. Am. Ceram. Soc.*, **97**, 2713, 2014; doi: 10.1111/jace.13165
[8] Musil J., Zenkin S., Kos S., Cerstvý R., Haviar S., *Vacuum*, **131,** 34, 2016; doi: 10.1016/j.vacuum.2016.05.020
[9] Musil J., *Surf. Coat. Technol.*, **125**, 322, 2000; doi: 10.1016/S0257-8972(99)00586-1
[10] Veprek S., *J. Vac. Sci. Technol.* A, **17**, 2401, 1999; doi: 10.1116/1.581977
[11] Miracle D.B., Senkov O.N., *Acta Mater.*, **122**, 448, 2017; doi: 10.1016/j. actamat.2016.08.081
[12] Gludovatz B., Hohenwarter A., Catoor D., Chang E.H., George E.P., Ritchie R.O., *Science*, **345**, 1153, 2014; doi: 10.1126/science.1254581
[13] Zou Y., Ma H., Spolenak R., *Nat. Commun*., **6**, 7748, 2015; doi: 10.1038/ ncomms8748
[14] Chen J., Zhou X., Wang W., Liu B., Lv Y., Xu D., Yang W., Liu Y., *J. Alloy. Compd.*, **760**, 15, 2018; doi.org/10.1016/j. jallcom.2018.05.067
[15] Rost C.M., Sachet E., Borman T., Moballegh A., Dickey E.C., Hou D., Jones J.L., Curtarolo S., Maria J.-P., *Nat. Commun.*, **6**, 8485, 2015; doi: 10.1038/ncomms9485
[16] Gild J., Zhang Y., Harrington T., Jiang S., Hu T., Quinn M.C., Mellor W.M., Zhou N., Vecchio K., Luo J., *Sci. Rep.*, **6**, 37946, 2016; doi: 10.1038/srep37946
[17] Pogrebnjak A.D., Postolnyi B.A., Kravchenko Y.A., Shipilenko A.P., Sobol O.V., Beresnev V.M., Kuzmenko A.P., *J. Superhard Mater.*, **37**, 101, 2015; doi: 10.3103/S1063457615020045
[18] Berardan D., Franger S., Meena A.K., Dragoe N., *J. Mater. Chem.* A, **4**, 9536, 2016; doi: 10.1039/C6TA03249D
[19] Fahrenholtz W.G., Hilmas G.E., *Scr. Mater.*, **129**, 94, 2017; doi: 10.1016/j. scriptamat.2016.10.018
[20] Vassen R., Cao X., Tietz F., Basu D., Stover D., *J. Am. Ceram. Soc.*, **83**, 2023, 2000; doi: 10.1111/j.1151-2916.2000.tb01506.x
[21] Lee T., Stanek C., McClellan K., Mitchell J., Navrotsky A., *J. Mater. Res.*, **23**, 1105, 2008; doi: 10.1557/jmr.2008.0143
[22] Grau-Crespo R., de Leeuw N.H., Hamad S., Waghmare U.V., *Proc. R. Soc. A*, **467**, 1925, 2011; doi: 10.1098/rspa.2010.0512

[23] Del Campo L., De Sousa Meneses D., Blin A., Rousseau B., V´eron E., Balat-Pichelin M., Echegut P., *J. Am. Ceram. Soc.*, **94**, 1859, 2011; doi: 10.1111/j.1551-2916.2010.04336.x
[24] Wang Z., Fang Q., Li J., Liu B., Liu Y., *J. Mater. Sci. Technol.*, **34**, 349, 2018; doi: 10.1016/j.jmst.2017.07.013
[25] Vegard L., *Z. Phys.*, **5**, 17, 1921; doi: 10.1007/BF01349680
[26] Zenkin S., Belosludtsev A., Kos S., Cerstvy R., Haviar S., Netrvalova M., *Appl. Phys. Lett.*, **108**, 231602, 2016; doi: 10.1063/1.4953262
[27] Hund F., *Z. Elektrochem. Angew. Phys. Chem.*, **55**, 363, 1951; doi: 10.1002/bbpc.19510550505
[28] Konusov F.V., Kabyshev A.V., Remnev G.E., *J. Surf. Invest.*, **5**, 228, 2011; doi: 10.1134/S1027451011030116
[29] Van Oss C.J., Good R.J., Chaudhury M.K., *Langmuir*, **4**, 884, 1988; doi: 10.1021/la00082a018
[30] Musil J., *Surf. Coat. Technol.*, **207**, 50, 2012; doi: 10.1016/j. surfcoat.2012.05.073
[31] Morscher G.N., Pirouz P., Heuer A.H., *J. Am. Ceram. Soc.*, **74**, 491, 1991; doi: 10.1111/j.1151-2916.1991.tb04049.x
[32] Toda-Caraballo I., *Scr. Mater.*, **127**, 113, 2017; doi: 10.1016/ j.scriptamat.2016.09.009
[33] Gild J., Samiee M., Braun J.L., Harrington T., Vega H., Hopkins P.E., Vecchio K., Luo J., *J. Eur. Ceram. Soc.*, **38**, 3578, 2018; doi: 10.1016/j.jeurceramsoc.2018.04.010
[34] Qi Z.B., Sun P., Zhu F.P., Wang Z.C., Peng D.L., Wu C.H., *Surf. Coat. Technol.*, **205**, 3692, 2011; doi: 10.1016/j.surfcoat.2011.01.021
[35] Pogrebnjak A.D., Yakushchenko I.V., Bagdasaryan A.A., Bondar O.V., Krause-Rehberg R., Abadias G., Chartier P., Oyoshi K., Takeda Y., Beresnev V.M., Sobol O.V., *Mat. Chem. Phys.*, **147**, 1079, 2014; doi: 10.1016/j.matchemphys.2014.06.062
[36] Moskovskikh D., Vorotilo S., Buinevich V., Sedegov A., Kuskov K., Khort A., Shuck C., Zhukovskyi M., Mukasyan A., *Sci. Rep.*, **10**, 19874, 2020; doi: 10.1038/s41598-020-76945-y